Novel Packaging Approaches for Increased Robustness and Overall Performance of Gimbal-less MEMS Mirrors

Veljko Milanović*, Abhishek Kasturi, James Yang, Yu Roger Su, Frank Hu
Mirrorcle Technologies, Inc., Richmond, CA

ABSTRACT

2D quasistatic (point-to-point) gimbal-less MEMS mirrors enable programmable, arbitrary control of laser beam position and velocity - up to their maximum limits. Hence, they provide the ability to track targets, point lasercom beams, and to scan uniform velocity lines over objects in laser imaging. They are becoming increasingly established in applications including 3D scanning, laser marking and 3D printing, biomedical imaging, communications, and LiDAR. With the increased utility in applications that demand larger mirror sizes and larger overall angle*diameter (θ*D) figures of merit, the technology is continuously pushed against its limit. As a result we have implemented mirrors with larger diameters including 5.0mm, 6.4mm, and 7.5mm, and have designed actuators with larger torque and angles to match the Θ*D demand. While the results have been very positive in certain application cases, a limitation for their more wide-spread use has been the relatively high susceptibility of large- θ*D mirrors to shock and vibrations. On the other hand, one of the challenges of MEMS mirrors of small diameters is their lower optical power tolerance simply due to their smaller area and heat removal ability. Although they can be operated at up to 2-3W of CW laser power, new developments in dynamic solid state lighting in e.g. headlights demand operation at up to 10W or beyond.

In this work we study and present several package-level approaches to increase mechanical damping, shock robustness, and laser power tolerance. Specifically, we study back-filling of MEMS packages with different gases as well as with different (increased) pressures to control damping and in turn increase robustness and useable bandwidth. Additionally, we study the effects of specialized mechanical structures which were designed and fabricated to modify packages to significantly reduce volumes of space around moving structures.

In their standard form and packaging the MEMS mirrors tested in this study typically measure quality factors of 75-100. Increases of pressure up to 50psi have shown relatively modest reductions of the overall quality factor to the 40-50 range. Backfilling of packages with heavier inert gasses such as Ar and SF_6 results in lowering of the quality factor down to 20-30 range. Mechanical modifications of the package with special structures and reduced air-gap to the window yielded the best results, reducing the quality factor to ~9-14. Combination of specialized packaging structures and gas backfill and pressure control could provide a very efficient heat transfer from the mirror and the desired near-critical damping, but has not been demonstrated yet. The increased performance does not change the compactness and low power consumption - the improved MEMS mirrors still consume <1mW. So far, designs with mirror sizes through 3.0mm diameter with increased damping have passed 500G shock tests.

In terms of improved heat removal we have found that the packaging improvement greatly increased optical power tolerance of MEMS mirrors from few Watts of CW laser power to >10 Watts. The exact numbers for the upper limit are not yet available - in samples where the heat removing structure was added and air was replaced with Helium, our setup with 3 combined lasers was not able to damage any samples.

Keywords: MEMS mirror, beam steering, 3D scanning, 3D imaging, MEMS damping, electrostatic combdrive actuators

1. INTRODUCTION

1.1 GIMBAL-LESS TWO-AXIS QUASISTATIC MEMS MIRRORS

Most of our gimbal-less MEMS mirror device types are designed and optimized for point-to-point or quasi-static optical beam steering [13],[1]. A steady-state analog actuation voltage results in a steady-state analog angle of rotation (tip/tilt positioning) of the mirror. At low frequencies or near DC, there is a one-to-one correspondence of actuation voltages and resulting angles: it is highly repeatable. All designs can be mechanically positioned to at least 16384 x 16384 clearly resolvable x-y mechanical positions. In other words, if a digital-based MEMS driving system with true, low-noise 14-bit voltage driving capability is attached to the MEMS mirror, the mirror could be commanded to 16384 measurably different and repeatable positions - on each of its two axes. In many cases that number is 20k x 20k or higher. As mentioned, a driver should have very low noise and high (e.g. 15-16 bit) precision to allow a system to achieve the

ultimate electromechanical capabilities of the MEMS mirror itself. It has been found that this repeatability does not have any measurable degradation over time in cases where the MEMS mirrors are packaged in clean/inert environments such as e.g. in hermetically capped TO-8 packages with dry N_2 backfill. Furthermore the performance is not degraded by the frequency of their use such as e.g. number of cycles. Billions of cycles are easily reached only in the first few months of a MEMS mirror's 10+ year lifetime. All of these key repeatability and reliability characteristics are owed to the pure single-crystal silicon design and construction and to the electrostatic actuation methodology. Namely the complete MEMS actuating structure is constructed in one single layer of a single-crystal silicon wafer. There are no special materials, piezoelectric, magnetic, or electrothermal. There are no significant currents running through structures, no metal interconnects in any flexures, and no magnets. Apart from single-crystal silicon structures and flexures there is only pad metallization and mirror metallization for high reflectance. For this reason our gimbal-less MEMS mirrors have been successfully used in applications at temperatures ranging from sub 1K (below -272.15°C) [16],[17] to around 473.15K (200°C) temperatures, though the standard operating range for most reliable operation is specified as -40°C to 105°C. Ultimately, any limitations are often related to the package and die-attach materials and adhesives rather than the MEMS chip itself.

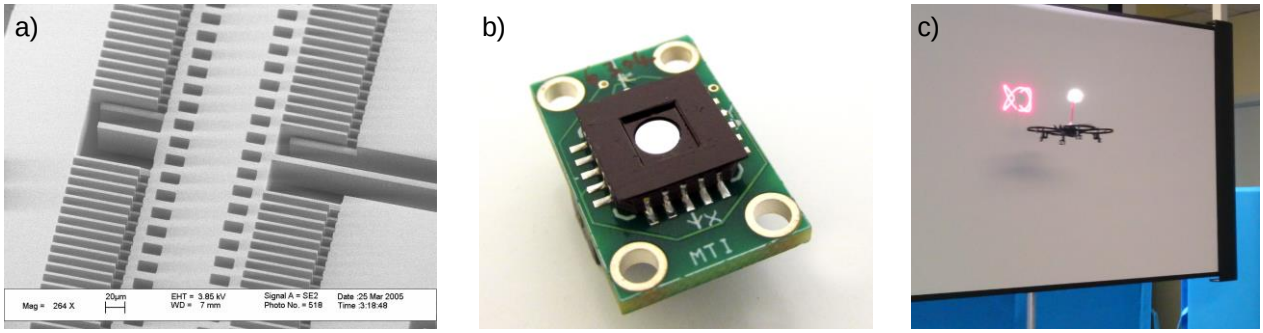

Figure 1. a) SEM image of the Multi-level beam vertical combdrive [8] which is the "motor" of each Gimbal-less two-axis MEMS mirror, b) A MEMS mirror of 3.0mm diameter in a connectorized package, with an aperture over the mirror instead of the standard AR-coated window, c) Tracking application where a MEMS mirror is pointing a laser beam at the small retro-reflective target mounted on a drone, and can track the drone's movements in two axes [6].

As mentioned, with the quasistatic capability, a sequence of actuation voltages results in a sequence of mirror angles for point-to-point laser beam-steering. Such devices can be operated over a very wide bandwidth from DC (maintaining position at constant voltage with nearly zero power consumption at the device) to several thousand Hertz with mechanical tilt range of -5° to +5° on each axis or larger depending on the design [1]. Such fast and broadband capability allows nearly arbitrary waveforms such as vector graphics, constant velocity line scanning, point-to-point step scanning, and resonant-quasistatic rastering (one axis resonant, the other quasi-static). These capabilities are utilized in established applications such as 3D scanning [2], biomedical imaging [3], free-space communication, LiDAR [4],[5], and laser tracking (Figure 1c) [6],[7]. At higher frequencies closer to device resonance, the full device response dynamics must be taken into account. A good approach to estimate "what will the MEMS mirror do if I apply the following waveform?" is to simulate or analytically assess the effect of the mirror's electromechanical transfer function on the specific waveform. Ultimately measurements give the final and most accurate answer but very good estimates can be obtained by relatively simple simulation.

The gimbal-less MEMS mirrors' actuators lend themselves inherently to a modular design approach. Firstly each actuator utilizes electrostatic combdrive rotators (Figure 1a) of designer-chosen length (depending on the allotted chip size). Our designs range from <1mm length rotators to ~9mm long rotators, and even special double-rotator designs to practically double the available torque on each side of the chip (Figure 2a and b). Furthermore, designer chooses arbitrarily stiff torsional supports for each rotator, arbitrarily stiff linkages between the rotator and the mirror, and arbitrarily positioned mechanical rotation transformers [10]. Those bi-axial flexures or rotation transformers which connect each rotator to the central mirror (or stage for bonded mirrors) determine the ratio of mirror angle to rotator angle which we call the angle gain. In addition, the device can have an arbitrarily large mirror diameter [1],[13] – however naturally not without significant trade-offs. Devices with larger-diameter mirrors are correspondingly quadratically slower due to the increased inertia. Namely, inertia of a round mirror plate is proportional to the fourth power of its radius and therefore the "speed" capability of the MEMS mirror is inverse proportional to the square its

radius. This is a general rule of thumb when comparing device designs, but many other parameters affect the actual performance especially die size and angle swing.

Integrated mirrors of 0.8mm, 1.2mm, 1.6mm, 2.0mm, and 2.4mm diameter are monolithically fabricated as an integrated part of the gimbal-less actuator device structure. They are the central area of the silicon die and share the same micro-fabrication steps as the surrounding electrostatic actuators. These mirrors are constructed of the same available silicon layers, featuring nearly perfectly flat and smooth silicon surfaces. On four sides, the mirrors are connected to bi-axial linkages that provide two-axis movement.

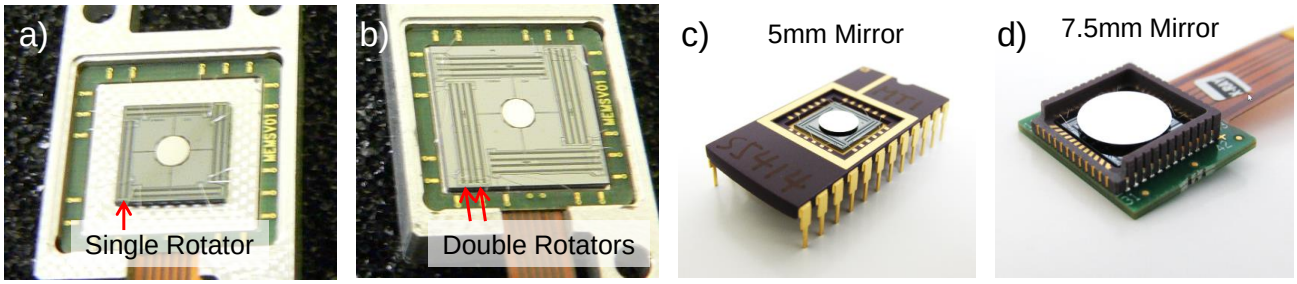

*Figure 2. a) A 8mm x 8mm MEMS actuator A4SR8.2-2400AL with a single rotator on each side, b) A 12mm x 12mm MEMS actuator A4DR12.2-2400AL with double rotators on each side of the chip, c) A4SR8.3-5000AL MEMS device with a 5.0mm mirror in a DIP24 package, providing +-5° of tip/tilt angle for a total θ*D factor of 25, d) A4QY8.4-7500AL MEMS device with a 7.5mm mirror, packaged in a customized ceramic on a rigid-flex carrier board – an experimental actuator, mirror and package design. This device provides +-7° of tip/tilt angle for a total θ*D factor of 52.5.*

Bonded mirrors are fabricated separately from the silicon actuator structure and are intended for subsequent micro-assembly on top of devices. Because these mirrors are attached from above the device actuator structure, they do not occupy a part of the actuator area and therefore can be essentially made in arbitrary sizes. The Bonded Mirrors methodology allows users to select the size up to 7.5mm diameter, as well as the geometry of mirrors for each individual application, in order to optimize the trade-offs between speed, beam size, and scan angle (Figure 2c and d).

1.2 PRIOR WORK ON DIELECTRIC-LIQUID ENHANCED MEMS

In 2016, we presented work demonstrating that MEMS mirrors can have dramatically increased performance in effective achievable resolution (θ*D product) when fully immersed and packaged in dielectric liquids with highly favorable torque-increasing, damping-increasing, and optical gain-increasing properties [14]. The rotating electrostatic combdrive had its torque multiplied by liquid's relative permittivity of ~2.5. Furthermore, by selecting the appropriate fluid viscosity, quality factor of the device was reduced and structural damping was tuned to near critical damping. Finally, the increased scan angle due to the ~1.5-1.7 index of refraction of the fluid was an additional benefit. These benefits of the fluidic packaging enabled us to double and in some cases triple the previously achieved θ*D product of two-axis quasistatic MEMS mirrors while still maintaining speeds applicable for above mentioned applications. For example, a standard MEMS mirror (A7B1.1-3000AL) with a 3mm diameter mirror and up to +-8° of mechanical deflection has a product of 24, while another (A4SR8.3-5000AL) with a 5mm diameter mirror and up to +-5° of mechanical deflection has a product of 25 (Figure 2c). Those could be increased ~1.5X in the cases of full immersion in dielectric liquid.

One of the most exciting benefits of the packaging methodologies is that the damping dramatically increases shock and vibration tolerance. While the results with MEMS actuators packaged fully immersed in dielectric fluids were very positive and exciting, there are obvious challenges related to reliably producing such packaging – without air bubbles, evaporation or leaks, etc. That work is ongoing and especially for some application areas that would most benefit from said figure of merit improvements.

1.3 GOAL OF THIS WORK

In this work, we investigate various other packaging approaches, without the above-mentioned dielectric liquids, which would still provide some of the mentioned benefits and would be more straightforward for productization. For example, we investigate specialized structures and gases in the MEMS mirror packages to increase the mechanical damping of the MEMS structures. The work consists of a three prong approach. The first is to add structures to the MEMS package, to

restrict the flow of gas surrounding the moving structures. The second approach is to replace the air (or N_2) filled package with higher density gases. The final approach is to increase the pressure within the cavity package. Potentially, a combination of all three approaches can be combined to create a highly optimized package to improve MEMS mirror performance by reducing Q, as well as increasing the mirror's heat dissipation capabilities.

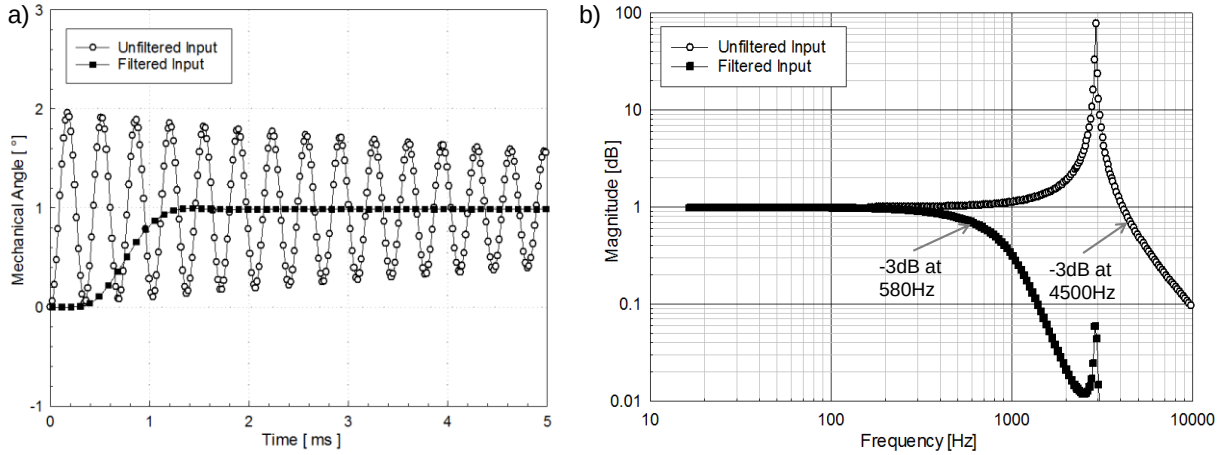

Figure 3. Typical responses of a 1.2mm diameter gimbal-less MEMS mirror in air, showing the challenge of the very high quality factor. a) step response of the MEMS mirror to unfiltered input vs. to input filtered with fc = fn/3, b) small-signal frequency response of the MEMS mirror with and without the filtered input.

One of the obvious consequences of this damping is a major increase in shock and vibration tolerance. Furthermore, driving of the MEMS mirror can be simplified without the need to cancel unwanted overshoot/ringing by multiple software and hardware methodologies. Namely, the very high quality factors of the silicon MEMS mirrors result in significant driving and controlling challenges. Since these are quasistatic or point-to-point beam steering devices, one of their most natural modes of operation is stepping from one position to another. In Figure 3 we see that the response of a typical gimbal-less MEMS mirror to a step function is an oscillation which can last for 10s of milliseconds or longer.

\MEMS mirrors manufactured in standard packages with air or N_2 backfill have quality factors (Q) as high as 100 (damping ratio of 0.005). This varies to some extent with mirror size and bonded vs. integrated mirror assembly approach but is always quite high. Due to this high Q, the unfiltered step waveform excites that resonance (2.91kHz in Figure 3b example) – so the beam overshoots to practically twice the desired angle, undershoots back to zero etc. This is clearly highly undesirable in any point-to-point beam-steering application. It should be noted that there are different considerations in cases where one of the axes or both axes are purposely allowed to oscillate at resonance in special raster scanning applications. However the focus of the work is on improving specifically broadband quasistatic performance and reducing any resonant response such as overshoot or ringing or shock-induced oscillation. Hence, what we often must do to avoid such overshoot and ringing is to pre-shape (in time domain) or filter (in frequency domain) the input waveform such that it does not excite the resonant peak which results in a relatively fast step settling time also seen in Figure 3a. But in order to get satisfactory results with a simple low-pass filter (here a 6^{th} order Bessel filter is used), we must set the cutoff frequency of the filter to approximately 1/3 of the resonant frequency (f_n) of that MEMS mirror. Figure 3b shows this filtered vs. original open loop response and we can see that indeed such a method suppresses the peak adequately but has a severe penalty in available bandwidth. The original -3dB point of the response was at 4500Hz and therefore with some optimal driving scheme that perfectly inverses the device responses all of that bandwidth would be available. However due to the need to pre-filter which is the simplest but often the only available solution in many applications, the -3dB point drops to 580Hz. It is evident then that any increased damping and therefore reduction of the Q-factor could allow a much more efficient utilization of the device's full available bandwidth, potentially allowing the use of the full bandwidth without the need for pre-shaping or filtering of command waveforms.

2. THEORETICAL APPROACH

2.1 SIMPLIFIED LINEAR MODEL OF THE INTEGRATED MEMS MIRROR

Here we consider a simple model for the gimbal-less two-axis MEMS mirror. The mirror's mechanical angle is proportional to the angle of driving rotators (rotating vertical combdrive actuators) [10], and the following discussion can be simplified and approximated by considering one complete axis sub-system of the gimbal-less two-axis MEMS mirror as an LTI second order system (Figure 5b). This approximation is for integrated (monolithic) MEMS mirrors [10]-[13] in which the mirror center of inertia is approximately in the same location as the (virtual) axis of rotation. It should be noted that in the following models we assume linearized driving of the MEMS mirror using the bias-differential quad-channel driving methodology [11].

The linearization is achieved by applying a Vbias voltage to all (opposing) rotator segments, and an additional Vdifference between opposing rotator segments to obtain proportional rotator position. Therefore the models assume Vdifference as the command input and mirror position as the output. The model can be expressed as shown in Figure 4a.

a)

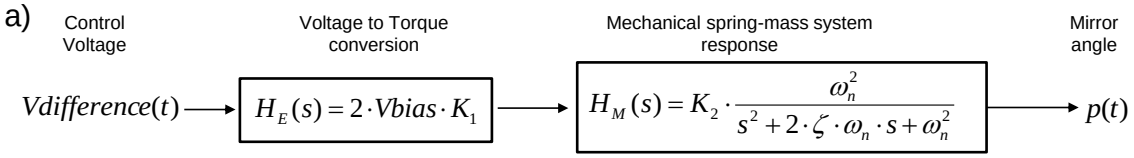

b)

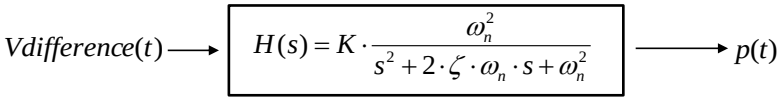

c)

Device	Diameter [mm]	K [°/V]	ζ (Zeta)	$\omega_n / 2\pi$ [Hz]	Vbias [V]
A3I8.2	0.8	0.0594	0.0067	3975	70
A3I12.2	1.2	0.0486	0.0067	2638	80
A1M16.5	1.6	0.0517	0.0067	1501	80
A7M20.1	2.0	0.0384	0.0067*	1314	80
A5M24.1	2.4	0.0459	0.0067*	850	80

Figure 4. a) A frequency domain model representing the integrated MEMS device as a 2nd order Linear Time Invariant system, with a voltage input and a MEMS mirror angle output, b) A simplified model of the 2nd order LTI system, c) A list of examples of integrated MEMS mirror devices that are represented by the 2nd order LTI system.

In the model we group various geometry and material-based constants as constants K_1 and K_2. The voltage to torque conversion constant K_1 is dependent on the size and shape of the electrostatic combdrive structure and the permittivity of the material between each individual comb finger in the combdrive. The mechanical response constant K_2 represents the mechanical compliance of the structure which defines the magnitude of mirror angle response with respect to a provided torque at the rotators. It is therefore the overall mechanical compliance of all the flexures but it also includes mechanical gain between rotator angle and mirror angle. In Figure 3b all those constant terms are grouped as a new constant *K* which provides for conversion from *Vdifference* input all the way to mirror angle *p*. The key parameters in the model then are as follows:

$$\mathrm{K} = 2 \cdot \mathrm{Vbias} \cdot K_1 \cdot K_2 \quad (1)$$

$$\omega_\mathrm{n} = 2 \cdot \pi \cdot f_n \quad (2)$$

$$\zeta = \frac{1}{2 \cdot \mathrm{Q}} \quad (3)$$

where K is the "voltage-to-angle gain" or mirror rotation per driver voltage (Figure 5a), ω_n is the undamped natural frequency of the system and ζ is the damping ratio. This 2nd order transfer function can very closely match the system plotted in Figure 5b. The primary goal is to modify the MEMS package, to increase the damping ratio ζ, and to see that the system response becomes more and more like an ideal wideband actuation system with full use of the natural -3dB bandwidth.

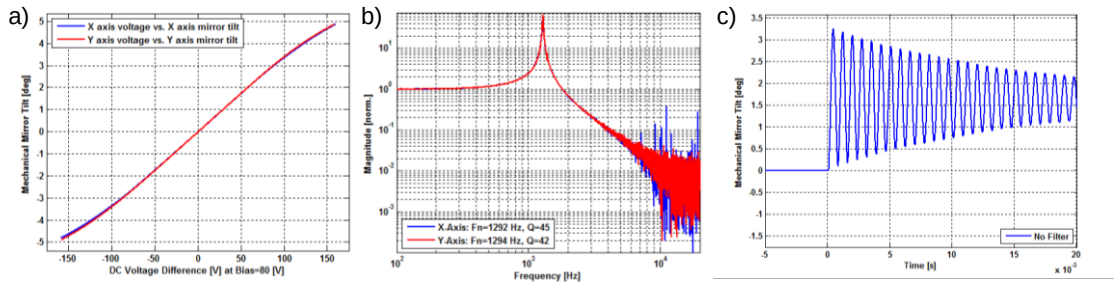

Figure 5. a) Voltage vs. Mechanical Angle graph, with the slope near 0 Voltage Difference representing the gain K, b) Frequency response of an Integrated MEMS device, represented as a LTI 2nd order system with 2 poles, c) Step response of an Integrated MEMS device, where no filtering was applied to the device, as a step of ~3° mech. angle is requested.

2.2 SIMPLIFIED LINEAR MODEL OF THE BONDED MEMS MIRROR

The simplified linear model for the bonded MEMS mirror has two additional orders than the integrated MEMS model. The bonded MEMS mirror and actuator system are represented as an LTI fourth order system (Figure 7b). The bonded MEMS mirror structure has a rotating MEMS actuator with a stage, and a mirror on a pedestal bonded to the actuator's stage. The two additional orders are from the mirror's center of inertia is no longer along the actuator, but above the plane of the actuator. These standard MEMS actuators are designed to accept bonded mirrors from 2.4mm up to 5.0mm diameter, coated with Aluminum or Gold. In special cases (experimental designs), 6.4mm and 7.5mm mirrors have been used with large-angle actuators as well. On the other end, there are other very stiff MEMS actuators designed with smaller mechanical angle range (e.g. A5L2.1 with +/-0.9°). Those MEMS actuators are often assembled with larger bonded mirrors above 5mm diameter. In R&D quantities we have demonstrated MEMS mirrors with 8mm and 9mm diameters on such high-stiffness actuators [1].

a)

Control Voltage — Mechanical spring-mass system response — Mirror angle

$$Vdifference(t) \longrightarrow H(s) = K \cdot \frac{\omega_{n1}^2 \cdot \omega_{n2}^2 \cdot (s+z_1)(s+z_2)}{(s+p_1)(s+p_2)(s+p_3)(s+p_4) \cdot \omega_{z2}^2} \longrightarrow p(t)$$

7 Parameters, K, ζ_1, ζ_2, ζ_z, ω_{n1}, ω_{n2}, ω_z

$$p_1 = -\omega_{n1}\zeta_1 - i\omega_{n1}\sqrt{1-\zeta_1^2} \qquad p_2 = -\omega_{n1}\zeta_1 + i\omega_{n1}\sqrt{1-\zeta_1^2}$$

$$p_3 = -\omega_{n2}\zeta_2 - i\omega_{n2}\sqrt{1-\zeta_2^2} \qquad p_4 = -\omega_{n2}\zeta_2 + i\omega_{n2}\sqrt{1-\zeta_2^2}$$

$$z_1 = -\omega_z\zeta_z - i\omega_z\sqrt{1-\zeta_z^2} \qquad z_2 = -\omega_z\zeta_z + i\omega_z\sqrt{1-\zeta_z^2}$$

b)

Device	Diameter [mm]	K [°/V]	$\omega_{n1}/2\pi$ [Hz]	$\omega_{n2}/2\pi$ [Hz]	$\omega_z/2\pi$ [Hz]	Vbias [V]
A8L1.1	3.0	0.0455	649	2024	1804	80
A7B2.1	2.4	0.0437	780	1462	1250	80

Figure 6. a) A simplified frequency domain model representing the bonded mirror MEMS device as a 4th order Linear Time Invariant system, with a voltage input and a MEMS mirror angle output, b) A list of examples of bonded mirror MEMS devices that are represented by the 4th order LTI system.

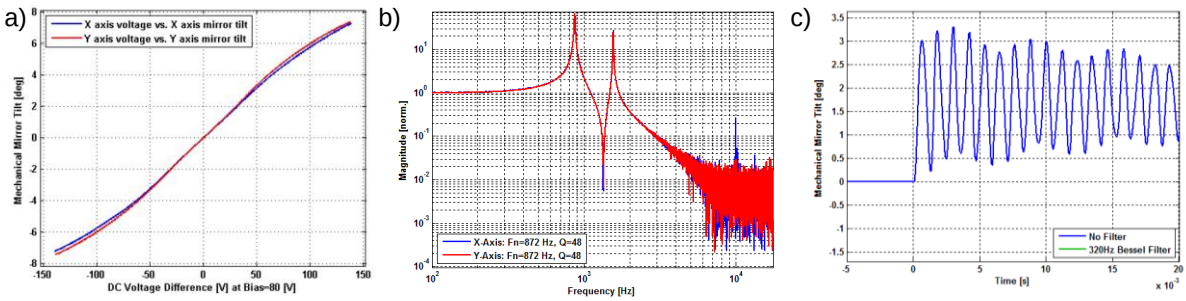

Figure 7. a) Voltage vs. Mechanical Angle graph, with the slope near 0 Voltage Difference representing the gain K, b) Frequency response of a bonded mirror MEMS device, represented as a LTI 4th order system with 4 poles and 3 zeros, c) Step response of a bonded mirror MEMS device, where no filtering was applied to the device.

2.3 QUALITY FACTOR REDUCTION

Quality factor in an oscillating resonator is the ratio of the energy stored to the energy dissipated by damping per oscillation cycle, and is (inversely) representative of the damping of the MEMS mirror. For resonators, a high quality factor results in larger displacements, SNR, reduced phase noise, and other benefits. Therefore there is quite a volume of published work on methods to increase quality factor of various types of MEMS resonators, e.g. inertial sensors, reference clock resonators, and resonant mirrors. In many cases such MEMS are used in vacuum to attain extremely high quality factors. But when driving a quasi-static MEMS mirror, the large quality factor results in undesirable overshoots and oscillations. In fact, the resonant peak of the quasistatic MEMS mirror is the one part of the response that we typically cannot use. It could be considered beneficial to have just that specific portion of the device response cancelled by appropriate driving or control methods such as with closed-loop control or inverse system filtering [12]. Furthermore, a high Q resonance in a mechanical structure like a MEMS mirror can make it highly susceptible to external environmental perturbation like from shock, vibration, and even sound. This is of concern both in use in terms of positional stability in a perturbing environment and also for overall survivability in major shock/vibe events. If the external perturbation includes frequency content in the vicinity of the high Q resonance the effect on the structure is magnified, sometimes catastrophically. Despite these multiple obvious benefits of increased damping in the category of MEMS which are to be operated in quasistatic mode, there are practically no publications discussing methods to increase damping.

2.4 IMPROVED HEAT REMOVAL FOR HIGH OPTICAL POWER APPLICATIONS

Since the mirror is quasi-static (point-to-point) capable and does not require vacuum for its operation like resonant-type MEMS mirrors [8], it benefits from considerable thermal conduction capability of the surrounding air in its package. This cooling-by-air capability is approximately proportional to mirror area, and therefore increases quadratically with mirror diameter. Prior work from a 2016 paper at SID has shown that the majority of thermal conduction from the mirror's surface is via conduction through the surrounding air [9]. That conduction is to the ceramic carrier below, to the surrounding anchored silicon structures, and to the glass window above. Hence the conduction is inverse proportional to the mirror's distance from those "cool" objects. Typically, the MEMS mirrors absorb 5% to 15% of the laser beam's energy (depending on the wavelength) with the standard Aluminum and Gold coatings. With these coatings, we have found that mirrors can be reliably operated at up to 2W of CW optical laser power in most wavelengths. At some specific wavelengths where reflectance is relatively higher, reliable operation is reached at powers as high as 4W (CW) even with mid-size (2mm diameter) mirrors. Finally, at 1064nm wavelength and with gold-coated 4.2mm and 5mm mirrors, operation at up to 10W of average optical power is reliable. Wavelength specific coated-mirrors showed higher reflectance to increase that range, but require a complex and costly deposition process.

Thus we explored two simpler routes to significantly increase this optical power tolerance without need for MEMS mirror re-design or metal coating alteration. One route was to design a new package in which distances between the mirror and cool reference surfaces are minimized. Above the mirror the fused silica window could be dropped from the standard height of 0.65mm above the mirror down to 0.15mm. Below the mirror we placed a custom-designed copper cooling structure, which minimizes distances to the mirror without mechanical interference at all possible mirror angles (5.5° on either axis and up to 7.75° on diagonals). This resulted in distance reduction from 0.45mm down to ~0.1mm.

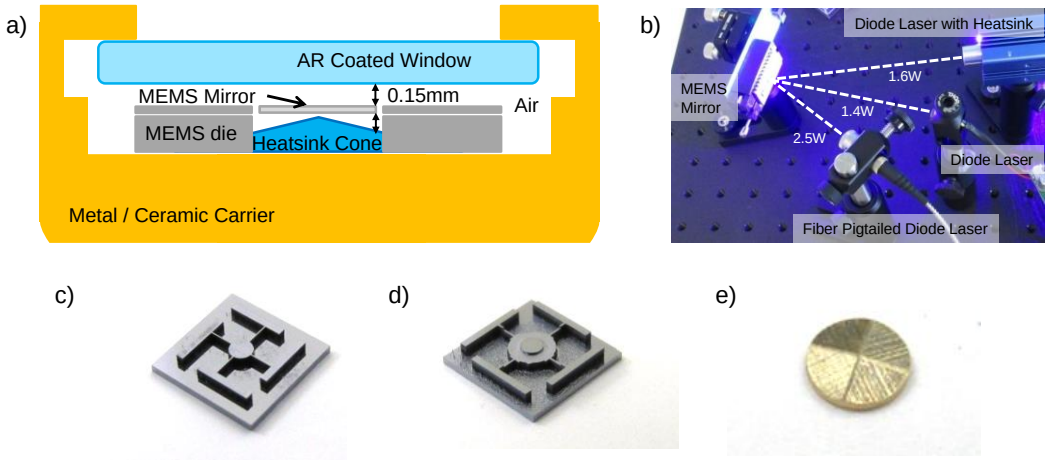

Figure 8. a) A MEMS package optimized for heat dissipation with a lowered window, and a heatsink cone beneath the mirror, b) MEMS mirror power handling test using three laser sources to achieve >5W of CW power, c) MEMS heatsink structure designed to fit under a MEMS actuator to fill in the cavities under the actuators, rotators and mirror, single level, d) Similar heatsink structure as figure c, with multiple levels to have the structure in the mirror cavity approach closer to the mirror, e) The simplest heatsink structure, a cylinder to fit under the mirror cavity, with the tip of the cone approach as close as possible to the backside of the mirror.

Since presenting our work in 2016, more complex cooling structures have been fabricated to reduce the volume of space near all moving structures of the MEMS device, and not just being limited to under the mirror cavity. Figure 8c shows a heatsink structure that goes under the MEMS actuator, covering up any backside openings, and reducing the space under the actuators, rotators and the mirror. Figure 8d is a more complex version of the structure in Figure 8c, with multiple layers, making portions of the structure move even closer to the MEMS mirror for increased thermal conductivity. Figure 8e is an image of the simplest structure, a cylinder with a pyramid structure on the top to have the center get as close as ~20µm to the center of tilt of the MEMS mirror, and the edges at an incline to match the maximum angle of the MEMS device. The pyramid structure on the top has the steepest of the inclines on the diagonals to accommodate the larger angles seen by the mirror when the both X-axis and Y-axis rotators are tilted to their maximum angle. With these two simple package modifications which nearly quadruple thermal conductance for the mirror we successfully operated multiple devices at the maximum available power of 5.5W (Figure 8b). We estimate >10W capability with these package improvements. The second route is to hermetically package the mirror in Helium environment. The combination of both approaches should result in 15W capability in full range of ambient temperatures.

3. EXPERIMENTAL SETUP

3.1 SELECTION OF MEMS MIRRORS

Three different MEMS device designs were selected for the study to improve overall performance using various pressures, backfilled gases and packaged structures around the MEMS mirrors. All three MEMS mirrors are designed for two-axis quasi-static (point-to-point) beam steering with ±5° mechanical tip/tilt angle and based on a gimbal-less, monolithic structure with vertical comb drive actuator design. The three MEMS devices are Aluminum coated, vary in mirror diameter and consequently the device bandwidth and resonant frequency. Additional designs were considered and used in selected tests but are not reported in this study since they did not go through all the tests. The additional devise include the A5M24.1 integrated MEMS mirror device with a 2.4mm Aluminum mirror, and the A8L1.1 actuator with a bonded 3.0mm Aluminum mirror. The selected designs for this study are:

MEMS Device Design	Mirror Diameter [um]	Chip Die Size [mm x mm]	Mechanical Angle* [°]	Resonant Frequency* [Hz]
A3I12.2	1200	4.25 x 4.25	+/-5°	2700
A1M16.5	1600	4.23 x 4.23	+/-5°	1500
A7M20.1	2000	5.20 x 5.20	+/-5°	1300

*Figure 9. A table of the three MEMS device designs used in this study. *Note: The mechanical angle and resonant frequency defined in the table are in standard, air-filled packages.*

3.2 SELECTION OF GASES

	Molecular Weight (g/mol)	Density (kg/m3)	Thermal Conductivity W/(m K)
Air	29.000	1.225	0.024
Helium*	4.003	0.164	0.151
Argon	39.948	1.633	0.018
SF_6	146.060	6.170	0.014

*Figure 10. A table of the gases selected for this study. *Note: Helium was considered for its high thermal conductivity properties but was not used due to immediate availability for our test setup.*

Argon (Ar) and Sulfur Hexafluoride (SF_6) were chosen as both gases are inert, have favorable optical properties and have densities greater than that of air. Argon has a density approximately ~1.5 that of air and SF_6 has a density approximately five times that of air and in both cases we expect higher damping. Helium was also considered and tested because it helps improve heat removal due to its high specific heat which helps keep the mirror cool. Based on immediate availability, only Ar and SF_6 were used in damping experiments, along with room atmosphere. Helium was used in experiments with high power lasers.

3.3 CHARACTERIZATION METHODOLOGY

Two stations were used to perform the characterization. For testing at different pressures, a device was placed in a 100PSI rated sealed chamber. The room atmosphere was then pumped into the sealed chamber, with a pressure gauge monitoring the pressure in the chamber for each increment of the test. For testing different gases, a device was sealed in a chamber and the chamber was backfilled with the gases to room pressure. Both stations used a 20mm x 20mm Position Sensitive Detection (PSD) used to measure the MEMS device's frequency response by reflecting a laser beam off the MEMS mirror to the PSD. A BDQ Amplifier connected to a NI-DAQmx card drives the MEMS device and observes the drive voltages and PSD output voltages. The measurements are used to characterize the MEMS device parameters such as frequency and step responses. The MEMS device is mounted with a ~20 degree of incidence from the CW laser and approximately 30mm away from the PSD, allowing the majority of the PSD to be used for measurement. The CW laser and PSD were not placed inside the sealed chamber for either of the two tests. The package modification tests were also performed on the same test station with the 20mm x 20mm PSD, NI-DAQmx card and BDQ Amplifier MEMS driver.

Before testing, the each MEMS device was fully characterized in our standard test, which includes voltage vs. angle gain, frequency response, step response, etc. However, while under test conditions, the voltage vs. angle relationship was not measured for tests in different gases or pressures as the permittivity change in the electrostatic combdrives is negligible, unlike in a dielectric fluid such as silicone oil. The measured frequency response is used to obtain an overall picture of the dynamic characteristics. To verify the resonant frequency and Q of the device, we fitted the step response to a model, and with the device's response in room atmosphere and pressure.

4. TESTS OF OPERATION AT INCREASED PRESSURES

The device under test is the A3I12.2, with 1.2mm integrated Al mirror. The device was first characterized in a room pressure environment to get a control baseline, and then inserted into a specialized chamber for the pressure tests. The pressure was gradually increased, and stopped at steps of 7.5PSI for a frequency measurement. As the pressure increases, the frequency response showed the MEMS device's resonance frequency slowly decreases, but no more than ~1.2%. The frequency response also showed that the Q at resonance drops almost in half at the highest tested pressure when compared to room pressure. Additional tests were scheduled to test devices at higher pressures, and with modified MEMS packages, but due to limited time and resources, only the A3I12.2 MEMS device was completely characterized. Initial results show that the MEMS device can benefit from a pressurized, hermetically sealed package.

a)

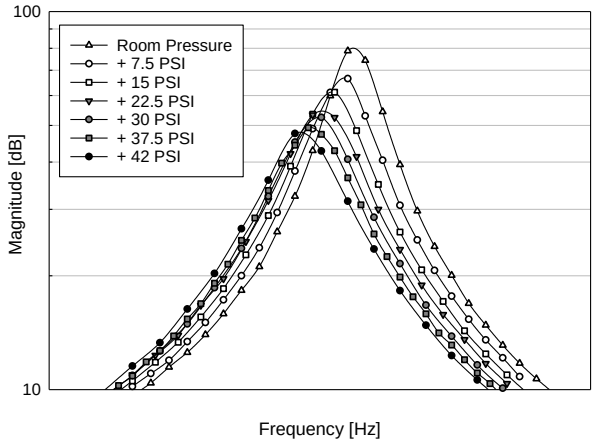

b)

Different Pressures at Room Temperature		
MEMS Device: A3I12.2		
Pressure	**Res. Freq. [Hz]**	**Q at Res.**
Room Pressure (~14 PSI)	2464	80
Room + 7.5 PSI	2456	69
Room + 15 PSI	2449	61
Room + 22.5 PSI	2446	56
Room + 30 PSI	2446	52
Room + 37.5 PSI	2439	49
Room + 42 PSI	2434	47

Figure 11. Pressure Results – a) Frequency Response of the A3I12 device on the PSD Test Setup at multiple pressures, b) a table of Resonant Frequencies and Quality Factors of the A3I12 device at multiple pressures.

5. TESTS OF OPERATION WITH DIFFERENT BACK-FILL GASES

The devices under test are the A3I12.2 and A1M16.5 integrated MEMS devices with 1.2mm diameter Al mirror and 1.6mm Al mirror respectively. The devices were first characterized in a room atmosphere environment to get a control baseline, and then inserted into a specialized chamber for the various gases. The experiment began by filling the chamber slowly with Ar gas, with multiple frequency response measurements taking place as the chamber transitioned from air to Ar. After the measurements were taken with the chamber filled with Ar gas, the chamber was cleared for the next experiment. The same procedure of filling the chamber and taking frequency response measurements was done when filling the chamber with SF_6. The results showed that Ar gas was able to significantly reduce the Q at resonance without affecting the resonant frequency. SF_6 meanwhile, shifted the resonant frequency left, slightly reducing it, but it also resulted in reducing the Q at resonance by at least half with the A1M16.5 device, and more than half the Q was reduced for the A3I12.2 device.

a)

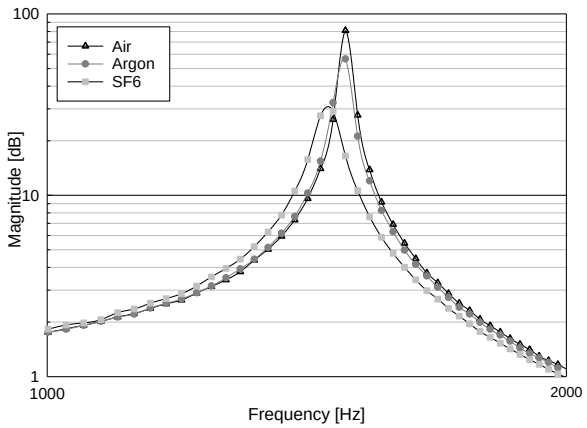

b)

Different Gases at Room Pressure		
MEMS Device: A1M16.5		
Gas	**Res. Freq. [Hz]**	**Q at Res.**
Air (N_2)	1487	82
Argon (Ar)	1487	56
Sulfur Hexafluoride (SF_6)	1454	31

c)

Different Gases at Room Pressure		
MEMS Device: A3I12.2		
Gas	**Res. Freq. [Hz]**	**Q at Res.**
Air (N_2)	2787	92
Argon (Ar)	N/A	N/A
Sulfur Hexafluoride (SF_6)	2753	56

Figure 12. Gas Backfill Results – a) Frequency Response of the A1M16.5 device on the PSD Test Setup with various gases, b) A table of Resonant Frequencies and Q of the A1M16.5 device with various gases, c) A table of Resonant Frequencies and Q of the A3I12 device with various gases.

6. TESTS OF OPERATION WITH MODIFIED PACKAGES

a)

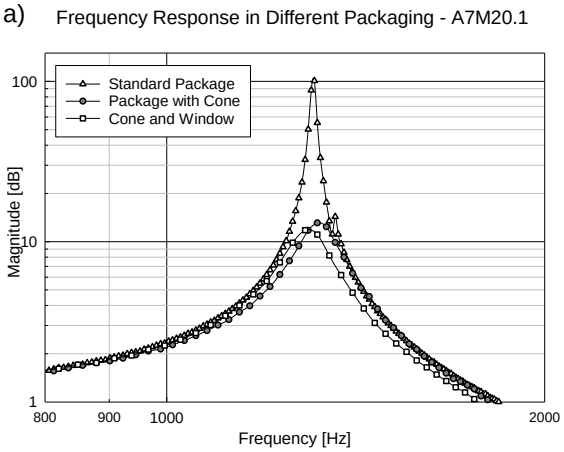

b)

MEMS Device in Package with Modifications		
MEMS Device: A7M20.1		
Package	**Res. Freq. [Hz]**	**Q at Res.**
Standard DIP24 Package	1309	110
DIP24 Package with Cone	1313	13
Package with Cone and Window	1294	12

c)

MEMS Device in Package with Modifications		
MEMS Device: A3I12.2		
Package	**Res. Freq. [Hz]**	**Q at Res.**
Standard DIP24 Package	2361	56
DIP24 Package with Cone	2312	12
Package with Cone and Window	N/A	N/A

Figure 13. Package Damping Results – a) Frequency Response of A7M20.1 device on the PSD Test Setup with package scale damping solutions, b) A table of Resonant Frequency and Q of A7M20.1 device with package scale damping solutions, c) A table of Resonant Frequency and Q of A3I12.2 device with package scale damping solutions.

Two package scale solutions we designed to reduce the Q at resonance by limiting the available volume of the atmosphere within the package cavity. A cone structure was placed underneath the MEMS mirror to reduce the air gap from ~450um to less than 100um which decreased the Q by a factor of 10. The second package scale solution was lowering the window to ~150um from the top of the MEMS mirror. Unlike the cone which is in a mostly enclosed cavity beneath the mirror, the window has gaps on all sides around the mirror that reduce its damping effectiveness which is why the Q changes minimally. A cross-section of this package is shown in Figure 8a. This packaging methodology yielded the best results, and in the future, this modified package can be combined with a different backfill gas, or pressured environment to further reduce the Q. In addition to the reduction of Q, this packaging methodology also increased the mechanical robustness of the MEMS device, enabling the device to survive higher shock tolerances when compared to the same device in a conventional package. This has so far been tested only informally by dropping various exposed device packages from different heights >1m onto the metal optical bench surface. In these informal tests the liquid-packaged MEMS have survived 100% of the time while air-packaged MEMS often broke.

7. MEMS PERFORMANCE AND QUALIFICATION TESTS

MEMS mirror designs considered and used in this study, as well as a few other designs were also tested with some standard environmental stress tests. To test mechanical robustness and life time, the MEMS devices were put to various tests to find the limits of the designs. One of the tests is fast ramp ("thermal shock") temperature cycling from -40°C to +125°C according to MIL-STD-883. All of the designs and all packaging varieties tested to date have always passed this test. Another test is mechanical vibration, variable frequency test, with 20G from 20Hz to 2kHz, according to MIL-STD-883 Method 2007 [15]. This test is again one that has not been found to challenge the devices or damage any. A further, more challenging test performed on the devices was a test of mechanical shock tolerance. The devices were tested to according to MIL-STD-883 Method 2002 [15], testing at six axes for 1ms shock at 500G peak and 0.5ms shock at 1500G peak. Additional (in-between) shock increments were added to the test since a wide range of MEMS devices were being tested, and we wanted to see how far certain designs were able to survive. The tests recorded shocks in X and Y-axis first, then a visual inspection is conducted on the devices to optically verify any structural damage, and the Z-axis shock is applied, followed by the visual inspection. The tests began with 300G shock tests, continued to 500G, 1000G and finally 1500G shock at the end. The results of the shock tests are shown in Figure 14. Note that none of the devices passed 1500G shock and therefore the line is not shown. The A5M24.1 MEMS devices in a modified package optimized for damping is shown as passed for 1000G shock, but not all the A5M24.1 devices passed this test in the Z-axis. Designs A3I12.1, A7M20.1 (with and without the damping structure), A5M24.1 (with and without the damping structure), and A8L1.1 with a bonded 3.0mm mirror all passed the 500G at 1ms shock.

MEMS	A3I12.2	A7M20.1	A7M20.1	A5M24.1	A5M24.1	A8L1.1
Mirror Dia.	1.2mm	2.0mm	2.0mm	2.4mm	2.4mm	3.0mm
Damping	No	No	Yes	No	Yes	No
300G Shock	Pass	Pass	Pass	Pass	Pass	Pass
500G Shock	Pass	Pass	Pass	Pass	Pass	Pass
1000G Shock	Pass	Fail	Fail	Fail	Pass*	Fail

Figure 14. A Table of the Shock Test Results – Most of tested devices passed the 500G tests but failed the 1000G tests A3I12 was able to pass the 1000G shock tests, and some of the A5M24.1 devices also passed the 1000G tests.

In addition to the performance qualifications presented, many MEMS devices manufactured over the past decade are still in operation in laboratory settings and in live applications of the technology. Recently, a life time test was put together to test cycles of operation of a MEMS device, operating at higher than rated voltages for the design. The test used four A5M24.1 integrated MEMS mirror devices, with a 2.4mm Aluminum mirror, in standard ceramic packages, scanning a sinusoid waveform at 140Hz, driven by 200V peak-to-peak. The standard A5M24.1 MEMS mirror is rated for 160V peak-to-peak, to reach a maximum angle of approximately +/-5.5° mechanical angle. The devices have been running continuously for +130 days, accumulating over 1.5 billion cycles of movement. The MEMS devices are checked daily for operation, and weekly under a microscope to check for any physical damage to the single-crystal-Silicon MEMS structure. These devices are operating in a clean laboratory setting and without any optical window or cover over the MEMS device. There has been some fine dust gathering along the edges of the MEMS mirror but it is not affecting the MEMS operation in any way.

8. CONCLUSIONS

Each of the individual tests yielded positive results. Increasing the pressure in the MEMS packages can reduce the Q, with a small effect on reduction of the resonant frequency. Backfilling the MEMS packages with various inert gases also saw a decrease in Q, and in some cases have additional benefits of increased thermal conductivity, meaning the MEMS mirror can work with higher laser powers. The MEMS package modifications produced the best results with the Q being reduced down to the 9-14 range. The modified package can be combined with a backfill of a gas can drastically increase the MEMS device's performance, and improve the mechanical structure to survive 500G shocks.

The changes in pressure and various backfill of gases does not change the compactness and low power-consumption of the MEMS-based beam-steering solution since the improved MEMS mirrors still consume <1mW in operation and drivers typically consume 100mW. The MEMS device can still be packaged in standard off-the-shelf packages such as TO-8, with an optically coated window cap to be hermetically sealed. The MEMS mirror package with PCB and its digital-input driver PCB are approximately 25mm x 25mm x 15mm in volume and weigh only <15g.

9. ACKNOWLEDGEMENT

The authors thank Dr. Daniel McCormick for assistance with MEMS characterization at elevated pressures. Additional thanks to Ping Hsu for assistance in finding manufacturers for the package-modifying metal points.

10. REFERENCES

[1] Mirrorcle Technologies, Inc. Website, Support Page 2016, http://mirrorcletech.com/support.html, March, 2016.

[2] Keshavmurthy, S.P., *et al*, "Non-contact Sensing System Having MEMS-based Light Source," Patent No. US20120062706 A1, March 15, 2012.

[3] Chen D. Lu, Martin F. Kraus, Benjamin Potsaid, Jonathan J. Liu, WooJhon Choi, Vijaysekhar Jayaraman, Alex E. Cable, Joachim Hornegger, Jay S. Duker, and James G. Fujimoto, "Handheld ultrahigh speed swept source optical coherence tomography instrument using a MEMS scanning mirror," Biomed. Opt. Express 5, 293-311 (2014)

[4] Moss, R., Yuan, P., Quesada, E., Sudharsanan, R., Stann, B., Dammann, J., Giza, M., Lawler, W., "Low-cost compact MEMS scanning ladar system for robotic applications", Proc. SPIE 8379, Laser Radar Technology and Applications XVII, 837903, May, 2012

[5] Spectrolab Website, SpectroScan 3D MEMS LIDAR System Model MLS 201 Datasheet, 2012, http://www.spectrolab.com/sensors/pdfs/products/SPECTROSCAN3D_RevA%20071912.pdf, March 2016.

[6] Milanović, V., Siu, N., Kasturi, A., Radojičić, M., Su, Y., ""MEMSEye" for Optical 3D Position and Orientation Measurement," Proc. SPIE 7930, MOEMS and Miniaturized Systems X, 7930-27, March, 2011.

[7] Richter, S., Stutz, M., Gratzke, A., Schleitzer, Y., Krampert, G., Hoeller, F., Wolf, U., Doering, D., "Position sensing and tracking with quasistatic MEMS mirrors," Proc. SPIE 8616, MOEMS and Miniaturized Systems XII, 86160D, March, 2013.

[8] Milanović, V., "Multilevel-Beam SOI-MEMS Fabrication and Applications," IEEE/ASME Journal of Microelectromechanical Systems, vol. 13, no. 1, pp. 19-30, Feb. 2004.

[9] Kasturi, A., Milanović, V., Yang, J., "MEMS Mirror Based Dynamic Solid State Lighting Module," Journal of the Society for Information Display, Display Week 2016, May 2016.

[10] Milanović, V., Matus, G., McCormick, D.T., "Gimbal-less Monolithic Silicon Actuators For Tip-Tilt-Piston Micromirror Applications," IEEE J. of Select Topics in Quantum Electronics, vol. 10, no. 3, pp. 462-471, Jun. (2004).

[11] Milanović, V. "Linearized Gimbal-less Two-Axis MEMS Mirrors," 2009 Optical Fiber Communication Conference and Exposition (OFC'09), San Diego, CA, Mar. 25, 2009.

[12] Milanović, V., Castelino, K., "Sub-100 µs Settling Time and Low Voltage Operation for Gimbal-less Two-Axis Scanners," IEEE/LEOS Optical MEMS 2004, Takamatsu, Japan, Aug. 2004

[13] Mirrorcle Technologies, Inc. Support Page, "Mirrorcle Technologies MEMS Mirrors – Technical Overview," http://mirrorcletech.com/pdf/Mirrorcle%20Technologies%20MEMS%20Mirrors%20-%20Technical%20Overview.pdf, March 2016

[14] Veljko Milanovic, Abhishek Kasturi, James Yang, " *Novel Fluidic Packaging of Gimbal-less MEMS Mirrors for Increased Optical Resolution and Overall Performance ,"* SPIE Defense and Commercial Sensing Conference 2016,Baltimore, MD, April 20th, 2016

[15] MIL-STD-883E Method-2002, "Test Method Standard – Microcircuits," 31 December, 1996. Dept. of Defense.

[16] R. Moffatt, "Two-Dimensional Spatial Imaging Of Charge Transport In Germanium Crystals At Cryogenic Temperatures", Ph.D. Dissertation, Stanford University, Mar. 2016.

[17] R. Moffatt et al., "Spatial imaging of charge transport in germanium at low temperature." Journal of Low Temperature Physics 176, 943–951, 2014